Coarse-Grained Simulation Studies of Effects of Polycation Architecture on Structure of the Polycation and Polycation–Polyanion Complexes

ARTICLE *in* MACROMOLECULES · OCTOBER 2012

Impact Factor: 5.8 · DOI: 10.1021/ma3011944

Macromolecules

Article

pubs.acs.org/Macromolecules

Coarse-Grained Simulation Studies of Effects of Polycation Architecture on Structure of the Polycation and Polycation–Polyanion Complexes

Robert M. Elder and Arthi Jayaraman*

Department of Chemical and Biological Engineering, University of Colorado, 3415 Colorado Avenue, UCB 596, Boulder, Colorado 80303, United States

Supporting Information

ABSTRACT: Polycations are a promising class of nonviral DNA delivery agents that bind to negatively charged DNA and transfect the DNA into target cells. The architecture and chemistry of the polycation strongly affect polycation–DNA complexation and in turn the ability of polycations to transfect DNA into cells. Here we develop coarse-grained models and conduct Langevin dynamics simulations to understand how the architecture of lysine-based polycations affects their complexation with DNA-like polyanions. We first characterize the structure of linear polylysine and oligolysines grafted to a polyolefin backbone and then the structure of complexes (termed polyplexes) formed by these polycations with polyanions of varying flexibility. We find that increasing oligolysine graft length and decreasing graft spacing both increase the size and rigidity of the grafted oligolysines, although they remain less rigid than semiflexible linear polylysine. Increasing ionic strength or counterion valency reduces polycation size and most architecture-dependent effects. The effects of polycation architecture on polyplex size and flexibility are dependent on the charge ratio in the system. Polyplex surface charge increases with increasing graft length or decreasing graft spacing.

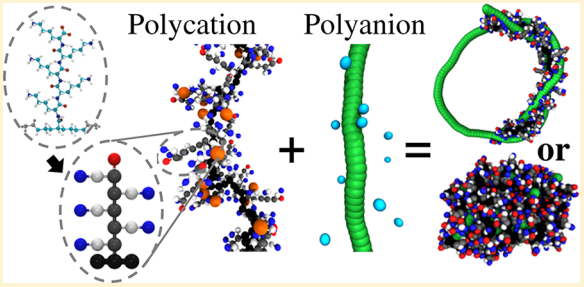

1. INTRODUCTION

Polyelectrolytes are chains of ionizable monomer units that impart periodic positive or negative charge along the chain in solution. The physical and chemical behavior of polyelectrolytes is quite complex due to interactions between these charges over multiple length scales. Understanding this complex behavior is of interest from both a fundamental and a practical standpoint. In particular, from a practical standpoint, polycations have been used as carriers, or vectors, for therapeutic gene delivery and are viewed as a preferred alternative to viral vectors, as polycations lack the immunogenic responses of the latter.[1,2] By forming compact, positively charged complexes (polyplexes) with polyanionic DNA or RNA, polycations allow therapeutic genetic information to cross the cell membrane and to be integrated into the genome.[1,2] A great deal of research effort has therefore gone toward synthesizing and characterizing polycations that maintain biocompatibility while approaching the high level of transfection efficacy inherent to viral gene delivery vectors.[3−7]

Previous experimental work has largely focused on designing polycations with novel chemistries and architectures to improve transfection efficiency.[3,5−8] Many polycations have been synthesized using combinatorial and rational approaches by varying the chemistry (e.g., polylysine,[4] polyamidoamine[9]) and architecture (e.g., linear,[3] branched,[10] comb-like[6]) of polycations and by introducing biocompatiblizing copolymers or proteins into the formulations, such as poly(ethylene glycol)[11] or an oligopeptide designed to target the nucleus.[6,7] One class of polycations recently synthesized and characterized by Emrick and co-workers shows striking architecture-dependent properties.[5−7] By reorganizing the structure of linear poly(L-lysine) (PLL) into a comb-like architecture of oligolysine grafted to a polyolefin backbone, poly(cyclooctene-*g*-oligolysine), the transfection efficiency was increased 50-fold over PLL, reaching levels that are comparable to the best commercially available transfection reagents.[7] Additionally, the stability of the polyplexes and transfection efficiency varied nonmonotonically with the length of the oligolysine grafts: polycations with intermediate-length grafts produced polyplexes with substantially higher transfection efficiency than polycations with either long or short grafts.[7] In recent work, we sought to explain the molecular and thermodynamic reasons behind the improved transfection efficiency of the grafted architecture over the linear architecture using atomistic molecular dynamics simulations and calculations of binding free energy.[12] We found that the polyolefin backbone in the grafted architecture weakens the free energy of polycation–DNA binding relative to linear PLL, which by improving polyplex dissociation within the cell could partially account for the improved transfection efficiency of the grafted architecture over the linear architecture. We also

Received: June 12, 2012
Revised: August 10, 2012
Published: September 19, 2012

dx.doi.org/10.1021/ma3011944 | *Macromolecules* 2012, 45, 8083–8096

matched the experimental trends in transfection efficiency as a function of architecture/graft length to trends in computationally obtained free energy of polycation−DNA binding as a function of architecture/graft length.[12] The nonmonotonic variation in free energy of binding with increasing graft length stems from a nonmonotonic trend in the entropy of binding, dominated by the counterion dissociation entropy.[12]

While the atomistic simulations were effective for studying the fine details of polycation−DNA binding, the atomistic resolution comes at the expense of limited length and time scales, making it infeasible to study the structure of full-sized polyplexes. In the present study, we have leveraged our knowledge of the atomistic behavior of the lysine-based polycations into a coarse-grained (CG) model where less-important details of the system are subsumed into fewer degrees of freedom, or "beads" that represent several atoms, allowing the study of greater length and time scales with reasonable computational expense. Using these coarse-grained models, we study how the architecture and flexibility of polycations affect the structure of polyplexes, which is not feasible with atomistic simulations.

There are some previous theory and simulation studies of polyelectrolytes that have examined the effect of architecture and flexibility on the structure of isolated polyelectrolytes and polyelectrolyte complexes. Linear uncharged polymers and charged polyelectrolytes of varying flexibility and charge density have been widely studied, both isolated in solution and forming complexes with oppositely charged polyelectrolytes.[13−16] A number of studies of grafted neutral polymers and charged polyelectrolytes (also referred to as comb-like or bottle-brush polymers depending on grafting density) have been reported, showing the effects of rigidity of various components,[17,18] spacing and length of the grafts,[19−21] the size of the monomers in the grafts,[22] and the hydrophobicity of the grafted backbone.[23,24] The effects of counterions on polyelectrolytes of varying architecture, both isolated in solution and complexed with an oppositely charged polyelectrolyte, have been explored.[13,23,25−28] Most of these previous coarse-grained computational studies have focused on model polyelectrolytes with architectures and interactions that are not connected to a specific chemical structure. In this paper we have sought to generate a simplified CG model that maintains several key features of three specific polycations: (1) linear poly(L-lysine) (PLL), (2) poly(cyclooctene-*g*-oligolysine) synthesized by Emrick and co-workers[5−7] which we denote as PCO-PolyX with X being the graft length, and (3) poly(cyclopentene-*g*-oligolysine) denoted as PCP-PolyX with X being the graft length. Specifically, the polycation CG model accurately mimics the relative sizes of the CG beads, the structure of the lysine monomers, and the graft length and graft spacing. The intrinsic rigidity of the peptide backbone in PLL and the oligolysine grafts is also accounted for, relative to the intrinsic flexibility of the grafted polyolefin backbone. For this study, the polyanion is a linear negatively charged chain of variable rigidity, modeled to mimic features of double-stranded DNA with each monomer representing a base pair.

We find using Langevin dynamics simulations with the above CG models how the architecture of the polycation—linear versus grafted, varying graft length, and varying graft spacing—affects the size, shape, and flexibility of the polycation and the polyplex formed with polyanions of varying flexibility. First, we study the linear and grafted architectures described above in both a charged state and a neutral state to isolate effects inherent to the architecture and effects due to electrostatic repulsion between adjacent grafts on the overall structure and flexibility of the polycation. Removing the charges from the linear semiflexible polycation results in a compact and flexible polymer, in agreement with what has been demonstrated previously for model polycations.[14,29] In the case of the grafted architecture, either increasing graft length or decreasing graft spacing increases the relative size and rigidity of the molecule. Removing the electrostatic effects, by eliminating charges from the grafted polycation, greatly reduces these architectural effects because of the greater range of electrostatic repulsion as compared to excluded volume repulsion. For both linear and grafted architectures, increasing the ionic strength or counterion valency can effectively neutralize the polycation charge and lead to behavior resembling that of the uncharged polymer, eliminating many architecture-dependent effects.

The size and shape of polyplexes formed by these lysine-based polycations with linear polyanions depend strongly on the polycation architecture, polyanion flexibility, and the positive-to-negative charge ratio (CR). In particular, polyplexes formed at charge neutrality (i.e., CR = 1, where the polycation charge exactly balances the polyanion charge) are small and globular in the case of fully flexible polyanion but are large and rod-like in the case of semiflexible, DNA-like, polyanion. For CR > 1, the polyplexes assume large, extended conformations for grafted architecture, but compact toroidal structures are observed for polycations with the longest grafts. The surface charge of the polyplexes is largely independent of the polyanion flexibility and depends mostly on polycation architecture and charge ratio: at CR = 1, all polyplexes possess neutral surface charge, but for CR > 1, the surface charge of the polyplex increases with increasing charge ratio, increasing graft length, or decreasing graft spacing. These results provide guidelines on how to tune the polycation architecture to modulate polyplex charge, size, and shape, which are important for processes like gene delivery involving polyplex transport into cells.

The remainder of this paper is organized as follows. In section 2, we describe the design and parametrization of our coarse-grained models, our simulation protocol, and the analysis methods we employ. In section 3.1, we characterize the behavior of the CG polycations in solution elucidating how polycation architecture, ionic strength, and counterion valency affect structure and flexibility of isolated polycations. In section 3.2, we characterize polycation−polyanion complexes (polyplexes) and relate polyplex size, shape, and surface charge to polycation architecture and the charge ratio. We conclude with a summary of results and implications of this work on future applications.

2. METHODS

2.1. Model Definition. We build and parametrize a coarse-grained model of lysine-based polymers in linear and grafted architecture by reproducing the key architectural features (the size, length, and spacing, and the flexibility) of various components in the polycations seen in our previous atomistic simulations[12] employing the Amber force field.[30] Additional atomistic simulations of poly(cyclopentene-*g*-oligolysine), beyond those included in our previous publication, also provide the basis for parametrizing our coarse-grained models. While the atomistic simulations used explicit TIP3P-model[31] water molecules, the coarse-grained model in this work takes into account the effects of water in an implicit manner and by doing so greatly reduces computational expense. We provide an

overview of the coarse-grained model here and additional details of the model development in Supporting Information section 1.

We model linear poly(L-lysine) (PLL) using three coarse-grained beads per lysine monomer (see Figure S1). The first bead represents the peptide link group ($-C(=O)NH-$). The two remaining beads represent the lysine α-carbon and R-group ($-CH(CH_2)_4NH_3^+$): the second bead represents the α-carbon, β-carbon, and γ-carbon atoms ($-CH(CH_2)_2-$), and the third bead represents the δ-carbon, ε-carbon, and charged amine group ($-(CH_2)_2NH_3^+$), as shown schematically in Figures S1 and S2. All hydrogen atoms are included in the bead that includes their parent heavy atom. Mapping the atoms in this manner results in approximately equal mass and size for the resulting CG beads, as shown in Table S1, and maintains the correct ratio of lysine monomer size to the spacing of the monomers, as shown in Figure S3. To model the negatively charged C-terminal ($-COO^-$) and the positively charged N-terminal ($-NH_3^+$) of the peptide backbone, a negatively charged bead is placed at one end of the peptide backbone, and a positively charged bead is place on the other end. The atoms comprising the C-terminal and N-terminal beads also have approximately the same mass and size as the other beads. To mimic the inherent rigidity of the peptide backbone, we calibrate a harmonic bending constant (k_{angle}, defined below) to impose an appropriate energetic bending penalty on the peptide backbone. We find that a value of k_{angle} = 30 energy/rad^2 best reproduces the atomistic results; the details of the procedure used to calibrate k_{angle} are available in Figure S4.

We also create coarse-grained models for two grafted polycations, poly(cyclopentene-*g*-oligolysine) and poly(cyclooctene-*g*-oligolysine). Throughout this work, we abbreviate the chemical name poly(cyclopentene-*g*-oligolysine) to PCP-PolyX, where X indicates the number of lysines in the oligolysine grafts; similarly, we abbreviate poly(cyclooctene-*g*-oligolysine) to PCO-PolyX. The only difference between the two grafted polycations is the number of carbon atoms in the backbone: PCP-PolyX has 5 carbon atoms, while PCO-PolyX has 8 carbon atoms. In the coarse-grained model of these grafted polycations, the three CG beads in the oligolysine grafts are the same as those in linear lysine described above, and a fourth bead type represents the polyolefin ($-(CH_2)_N-$) backbone. The atoms comprising each polyolefin backbone bead depend on the chemical structure of the backbone: for the pentene backbone in PCP-PolyX the five methylene groups ($-(CH_2)_5-$) are divided equally among two identical CG beads, while for the octene backbone in PCO-PolyX the eight methylene groups ($-(CH_2)_8-$) are divided equally among three identical CG beads. Regardless of the length of the polyolefin backbone, the properties of the polyolefin backbone beads are identical. The mass and size of the polyolefin backbone bead are similar to the beads defining the linear lysine model. Choosing three polyolefin backbone beads to represent octene and choosing two beads to represent pentene maintains the ratio of graft length to graft spacing seen in atomistic model, as shown in Table S2. The polyolefin backbone is completely flexible (k_{angle} = 0 energy/rad^2) and has the same van der Waals well depth as all other species. These choices are justified based on comparing the results of extensive coarse-grained simulations with atomistic simulation results, as detailed in Supporting Information section 3. The oligolysine grafts are bonded to the second bead of every polyolefin backbone monomer, which each consist of 2 or 3 beads as mentioned above. The grafts possess a negatively charged C-terminal CG bead, but grafting to the polyolefin backbone eliminates the positively charged N-terminal.

We model a DNA-like polyanion using a simplified 1-bead coarse-grained model where each bead represents a single DNA base pair. Each CG bead has a valency of 2, corresponding to the two negatively charged phosphate groups in each base pair. The mass of these beads is chosen to be 6.3 times the unit mass because the ratio of the average mass of a DNA base pair (263 g/mol) is 6.3 times our basis for the unit mass (41.8 g/mol). The distance between the beads is chosen to replicate the distance of 3.4 Å between consecutive base pairs, and the radius of the polyanion beads is 6.7 Å, a choice we discuss in Supporting Information section 4. Finally, to parametrize the stiffness of the DNA backbone, we conducted a series of simulations of an uncharged CG 1-bead polymer with varying bending coefficient (k_{angle}, defined below), from which we determined that a value of k_{angle} = 460 energy/rad^2 best duplicates the DNA persistence length of ~50 base pairs in the high salt limit.[32] Specifics of this procedure are given in Figure S5.

Mobile ions are modeled as charged spheres. In all cases, the positive and negative counterions have the same valency, either they are both monovalent or they are both divalent. Because of the level of coarse graining, it is not possible to assign a specific chemical identity to the counterions. Several possible biologically relevant mobile ions (e.g., Na^+, Mg^{2+}, Ca^{2+},Cl^-, SO_4^{2-}, etc.) and the rationale for choosing the mass and van der Waals parameters of the counterions are listed in Supporting Information section 1.

2.2. Unit Definitions and Model Interactions. All units in our simulations are dimensionless and can be connected to physical quantities through the definitions of unit mass, unit length, and unit energy. We define unit mass as 41.8 g/mol, the average mass of the atoms comprising the polycation beads, unit length σ as 3 Å, the approximate average end-to-end distance of the atoms making up the polycation beads, and unit energy ε as 0.1 kcal/mol, a representative Lennard-Jones well depth of the atoms making up the polycation (excluding hydrogen), as defined in the Amber force field.[30]

A harmonic potential is applied between bonded coarse-grained beads in both the polycation and polyanion

$$U_{bond} = k_{bond}(r - r_0)^2 \quad (1)$$

where k_{bond} is the equilibrium constant and r_0 is the equilibrium bond length. k_{bond} is chosen as 500 ε/σ^2 such that the standard deviation around the equilibrium distance is ~10%, which prevents bonds from nonphysically intersecting one another. The equilibrium bond lengths are all 1σ, except for a bond length of 1.1σ between DNA beads. Angular constraints are applied using a harmonic potential:

$$U_{angle} = k_{angle}(\theta - \theta_0)^2 \quad (2)$$

where k_{angle} is the equilibrium constant and θ_0 is the equilibrium angle. As noted earlier, for the peptide backbone k_{angle} = 30 ε/rad^2 and for the semiflexible, DNA-like polyanion k_{angle} = 460 ε/rad^2, and $\theta_0 = \pi$ in both cases. k_{angle} is zero in all other cases. van der Waals interactions between all CG beads are described using the Lennard-Jones potential:

$$U_{LJ} = 4\varepsilon_{LJ}\left[\left(\frac{\sigma}{r}\right)^{12} - \left(\frac{\sigma}{r}\right)^{6}\right] \quad (3)$$

dx.doi.org/10.1021/ma3011944 | Macromolecules 2012, 45, 8083−8096

where ε is the well depth, σ is the location of the energy minimum, and r is the distance between two CG beads. The well depth of $\varepsilon_{LJ} = 0.6\varepsilon$ is chosen for all CG beads because it produces physically reasonable behavior (e.g., the linear polycation maintains the same conformation as in the atomistic case), where ε is the unit energy defined above. The polyolefin backbone could be considered hydrophobic based on its chemical nature and thus might require a stronger self-attraction and higher value of ε_{LJ} to mimic solvent effects. However, we find that hydrophobicity of the polyolefin backbone is not a major factor in dictating the structure and flexibility of the polyelectrolytes in our system, and therefore the value of ε_{LJ} between the polyolefin backbone beads is also 0.6ε. The location of the energy minimum, σ, for a given pair of beads is chosen as the sum of their radii. Electrostatic interactions are calculated using the Coulomb equation

$$U_{Coul} = \frac{q_i q_j}{\varepsilon_r r_{ij}} \tag{4}$$

where ε_r is the relative permittivity of the implicit solvent (defined as 80 here to mimic water at 300 K), q_i is the charge of the ith particle, and r_{ij} is the distance between the particles i and j. No dihedral or improper torsion terms are used in these models.

2.3. Simulation Protocol. We conduct Langevin dynamics simulations of the models described above using the LAMMPS package.[33] Langevin dynamics are defined by the equation

$$F = -\nabla U(\vec{r}) - \frac{m}{\gamma}\vec{v} + \sqrt{\frac{k_B T m}{\gamma\, dt}}\, R(t) \tag{5}$$

The first term originates from classical dynamics (the negative gradient of the potential), the second term represents friction between the particle and the implicit solvent, and the third term represents a random acceleration term due to collisions with the implicit solvent molecules. F is the force on a particle, U is the potential (defined by the positions r of all the particles), m is the particle mass, γ is the friction coupling coefficient, v is the particle velocity, k_B is the Boltzmann constant, T is the temperature, and R is a random number function with Gaussian distribution.[34]

Our simulation protocol consists of two steps. First, the energy of the initial system configuration is minimized to a root-mean-square (rms) gradient of 10^{-4} to remove any highly unfavorable contacts, which typically requires less than 1000 steps of conjugate gradient minimization. Then, after assigning initial velocities based on a Boltzmann distribution around the desired temperature, Langevin dynamics are carried out for 10^7 time steps, which we find is sufficient time for these systems to reach and sample their equilibrium state. The particle−particle particle−mesh (PPPM) method is used to calculate the electrostatic interactions, with a real space cutoff of 20σ, a tolerance of 10^{-2}, and an interpolation order of 2.[35] The parameters for the PPPM method, which is closely related to the particle−mesh Ewald (PME) method, are chosen based on performance considerations and by showing that energy is conserved with these choices aside from fluctuations due to the Langevin thermostat. van der Waals interactions are cut off at 10σ, and the CHARMM switching function is applied up to 12σ. The Langevin friction coefficient, γ, is 5 (in dimensionless time units), and the dimensionless temperature, T^*, is 6, which roughly corresponds to 300 K. A physically reasonable value for the damping coefficient is estimated by assuming a diffusion coefficient of 5×10^{-7} cm^2/s, roughly corresponding to a large DNA molecule in water, and using the relation $\gamma = Dm/(k_B T)$, where D is the diffusion coefficient, m is the particle mass, and $k_B T$ is the thermal energy; with our bead mass of 41.8 g/mol; this calculation results in the drag coefficient of 5. The time step is 0.0075 dimensionless time units. The box size is $(100\sigma)^3$ for isolated polyelectrolytes and $(300\sigma)^3$ for systems modeling polycation−polyanion condensation, and the boxes are periodic in three dimensions.

Initial configurations of the polycations and polyanions are generated in helical configurations with parameters of the helices chosen to make the initial configurations relatively compact and to avoid undesirable steric clashes at the beginning of a simulation. Note that this helical configuration is merely for convenience and is unrelated to the structure of DNA. Counterions are placed randomly near the polyelectrolytes. In systems including both polycation and polyanion, the points for generating the helical polyelectrolyte initial structures are placed $\sim 150\sigma$ apart so that the polyelectrolytes are initially as far apart as possible.

2.4. Parameters Varied. For the linear architecture, we simulated polycations with following number of monomers: 24, 32, 40, 48, 72, 96, 120, 144, 196, and 240. For the grafted architecture, we simulated polycations with all combinations of the following parameters: graft lengths of 2, 3, 4, or 5 lysines; graft spacings of 2 (PC**P**-PolyX) or 3 (PC**O**-PolyX); and polycations with 8, 24, 48, or 72 monomers. All of these polycations are simulated at multiple ionic strengths: neutralizing (i.e., with only the number of counterions required to neutralize the polycation charge, which we denote as "neutral"), 50 mM, and 100 mM. Counterions are either monovalent or divalent. We also conducted simulations of all of these polycation architectures with all beads having no charge and in the absence of counterions.

Simulations of polycation−polyanion complexation are conducted with either fully flexible or semiflexible polyanion with 200 beads. Polycation−polyanion complexation simulations are conducted with all of the aforementioned polycation architectures: linear and grafted with graft lengths of 2, 3, 4, or 5 and graft spacing of 2 or 3. The ratio of positive to negative polyelectrolyte charge (which we denote as charge ratio CR) is varied by changing the length of the polycation to achieve the following values of charge ratios: 0.5, 1.0, 1.5, and 2.0. In polycation−polyanion complexation simulations, neutralizing monovalent counterions for both polyelectrolytes are included: a constant 400 positively charged counterions to balance the charge of the polyanion and a variable number of negatively charged counterions to balance the charge of the polycation.

2.5. Analysis. We have chosen a variety of methods to characterize the structure of the polycations. We calculate the end-to-end distance, R_{ee}, the average distance between the first and last monomers in a polymer, and the radius of gyration, R_g, the average distance of the monomers from the center of mass (R_{com}) of the polymer, defined by the equation

$$\langle R_g^2 \rangle = \frac{1}{N}\left\langle \sum_{i=1}^{N} (R_i - R_{com})^2 \right\rangle \tag{6}$$

where N is the number of monomers and R_i is the position of monomer i. Angular brackets denote ensemble averages. Both R_{ee} and R_g vary with the length of a polymer in characteristic scaling relationships defined as $R \propto N^{\nu}$, where R may be R_{ee} or R_g, N is the number of monomers, and ν is termed the scaling

dx.doi.org/10.1021/ma3011944 | Macromolecules 2012, 45, 8083−8096

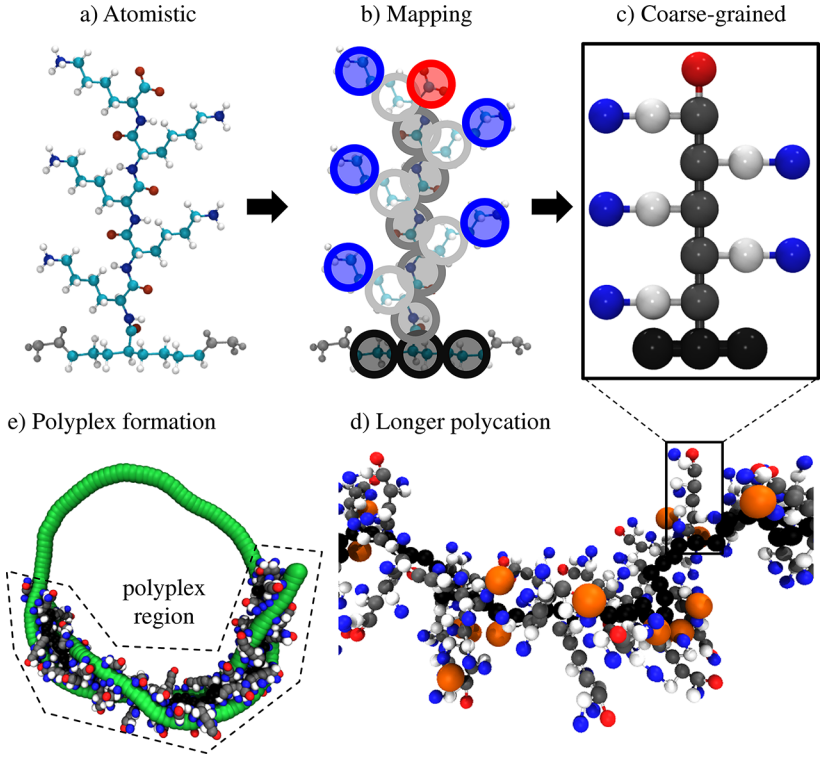

Figure 1. Schematic of the coarse-grained polycation model. The atomistic structure (a) pictured is poly(cyclooctene-*g*-pentalysine), PCO-Poly5. The overlay of transparent circles in (b) qualitatively demonstrates the correspondence of the atomistic structure to the final coarse-grained structure (c). A representative snapshot of a PCO-Poly5, including counterions (larger spheres), is shown in (d). An example snapshot of a polyplex and a diagram of the polyplex region are shown in (e). Figure S1 shows a similar diagram of our model of linear poly(L-lysine).

factor. Scaling factors are determined from the slope of a log−log plot of R versus N. Notable examples of scaling factors are $\nu = 1/3$ for a sphere, $\nu = 0.588$ for a self-avoiding random walk, and $\nu = 1$ for a rigid rod. Therefore, flexible polymers in a globular shape have approximately $\nu = 0.6$, whereas more rigid-rod-like polymers approach $\nu = 1$.[36] In this work, we report the radius of gyration of only the backbone of the polymer (either peptide in the case of linear polycation or polyolefin in the case of grafted polycation).

We also calculate the ratio of the above quantities, R_{ee}^2/R_g^2, a measure of the shape of a polymer. While values of $R_{ee}^2/R_g^2 \sim 12$ typically indicate a rod-like conformation, values near 6 indicate a globular conformation resembling a random walk. Finally, the ratio of R_{ee} to the contour length, R_{max}, gives an indication of how stretched or coiled the polymer is. R_{max} is the maximum distance between the first and last monomers of the chain if it is in a perfectly linear conformation with the bonds at equilibrium distances.[36]

Another measure of the shape of a polymer is the relative shape anisotropy (RSA). To calculate the RSA, we first calculate the radius of gyration tensor, $T_{\alpha\beta}$, which is defined by

$$T_{\alpha\beta} = \frac{1}{N}\sum_{i=1}^{N}(R_i - R_{com})_\alpha (R_i - R_{com})_\beta \tag{7}$$

where α and β denote the three Cartesian directions x, y, and z. The three eigenvalues of $T_{\alpha\beta}$, calculated by diagonalizing the gyration tensor, are denoted as λ_1^2, λ_2^2, and λ_3^2 and having the relation $\lambda_1^2 \geq \lambda_2^2 \geq \lambda_3^2$.[37] These eigenvalues, which sum to the radius of gyration squared, are the magnitudes of the eigenvectors pointing along the three principal axes of the structure in question. From these three eigenvalues, we compute the asphericity, A_S:

$$A_S = \lambda_1^2 - \frac{1}{2}(\lambda_2^2 + \lambda_3^2) \tag{8}$$

which is 0 for a perfect sphere. We also compute the acylindricity, A_C:

$$A_C = (\lambda_2^2 - \lambda_3^2) \tag{9}$$

which is 0 for a cylindrically symmetric structure.[38] Finally, the RSA is computed as

$$\mathrm{RSA} = \frac{A_S^2 + 0.75A_C^2}{R_g^4} \tag{10}$$

which is bounded between 0 (for a perfectly isotropic structure, such as a sphere) and 1 (for a perfectly anisotropic structure, such as a rod).[38]

A measure of the local flexibility, as opposed to the global values that arise from the ratio R_{ee}^2/R_g^2 and the RSA, is the orientational correlation function. We have chosen two ways to examine the orientational correlation. The first is the scalar projection of each bond in the polymer onto the first bond, defined mathematically by

$$\langle \cos(\theta)\rangle^k = \langle \vec{b}_0 \cdot \vec{b}_k \rangle \tag{11}$$

where b_k is the kth bond vector and the dot indicates the scalar product. This value is a function of the position along the polymer, k, and begins at a value of 1 at $k = 0$ followed by a decay with increasing k. The manner of the decay can be indicative of a particular type of polymer. For example, the

dx.doi.org/10.1021/ma3011944 | *Macromolecules* 2012, 45, 8083−8096

wormlike chain (WLC) model of semiflexible polymers decays exponentially with a characteristic length known as the persistence length.[36] However, polyelectrolytes and flexible polymers are not well described by a simple exponential decay, and we do not focus on the standard WLC definition of the persistence length.[39,40] Our second way of quantifying the orientational correlation is the scalar projection of the end-to-end vector onto each bond in the polymer. This is defined mathematically by

$$L_p{}^k = \langle \hat{b}_k \cdot \hat{R}_{ee} \rangle \tag{12}$$

where circumflexes indicate unit vectors. Unlike the typical WLC exponential decay definition of the persistence length, the quantity $L_p{}^k$ does not assume a uniform persistence length and instead provides a local persistence length at each bond, which is more appropriate for flexible chains.[21]

To examine the location and effect of counterions on the polymers, we calculate the number and fraction of counterions adsorbed to either the isolated polyelectrolyte or the polyplex, both the total number adsorbed and the number adsorbed to each monomer. Counterions are defined as "adsorbed" when they are within the Bjerrum length of the corresponding oppositely charged bead on the polyelectrolytes. The Bjerrum length is the ratio of the attraction of two point charges to the thermal energy. The Bjerrum length in dimensionless units is defined as

$$\lambda_B \equiv \frac{e^2}{\epsilon_r k_B T} \tag{13}$$

where e is the unit charge, ε_r is the dielectric of the medium, and k_BT is the thermal energy. Using this equation and our simulation parameters yields a Bjerrum length of 2.3σ. This is equal to the Bjerrum length in water at 300 K, ~7 Å, divided by our unit length of 3 Å/σ, providing a consistency check for our system of dimensionless units. In cases where a counterion is within the Bjerrum length of multiple monomers, we consider it to be bound to only the closest monomer, which eliminates double counting of counterions.

For all calculations on polyplexes, we consider only the region where the two polyelectrolytes are within the Bjerrum length of each other, which is termed the polyplex region in the discussion below. For instance, the radius of gyration of the polyplex includes only the polycation beads that are within the Bjerrum length of a polyanion bead and the polyanion beads that are within the Bjerrum length of a polycation bead, and these beads are considered the polyplex region, which is shown schematically in Figure 1e. Finally, we calculate the counterion-accessible surface area of the polyplex region using the VMD built-in measure command with a probe radius of 1σ, which is the diameter of the counterions in our simulations.[41]

3. RESULTS AND DISCUSSION

3.1. Polycation Structure. *3.1.1. Effect of Polycation Architecture and Charge.* First, we consider the effect of architecture and charge on the size, shape, and local and global flexibility of the lysine-based polycations with only neutralizing counterions. Figure 2a shows the radius of gyration of the backbone of the linear and grafted polycations. R_g increases with the number of monomers, N, in the characteristic power-law behavior of polymers, which is evident from the linear nature of the relationship on a log−log plot. At constant N, the linear polycation is the smallest, PCP-PolyX is intermediate in size, and PCO-PolyX is the largest. This trend is expected because for a constant number of monomers N the number of backbone beads in each monomer increases from linear (1 bead per monomer) to PCP-PolyX (2 beads per monomer) to PCO-PolyX (3 beads per monomer); thus, the overall sizes of the polymers also increase. As graft length (X) increases R_g increases but with decreasing returns, with the size difference between PCP-Poly2 and PCP-Poly3 being greater than the size difference between PCP-Poly4 and PCP-Poly5; the same trend is also observed for PC**O**-PolyX. The effect of increasing the graft length on polycation size decreases as the graft length increases because each added lysine on the graft has a larger free volume than the previous lysine in the graft, and therefore the lysine repels neighboring grafts less strongly.

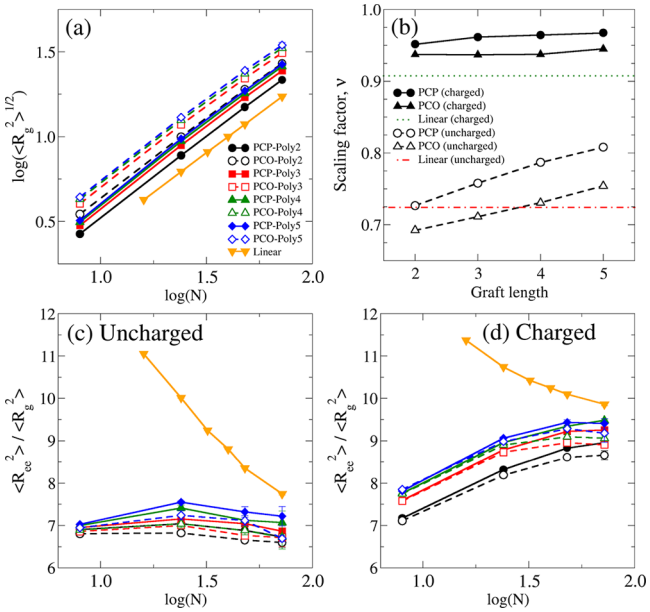

Figure 2. Effect of architecture and charge on polycation structure. (a) $\langle R_g^2 \rangle^{1/2}$ as a function of number of monomers, N. (b) The scaling factor, ν, from the relation $R_g \propto N^{\nu}$. (c) The ratio $\langle R_{ee}^2 \rangle / \langle R_g^2 \rangle$ for uncharged polymers. (d) The ratio $\langle R_{ee}^2 \rangle / \langle R_g^2 \rangle$ for charged polycations. Panels a, c, and d share the same legend.

Figure 2b shows the scaling factors, ν, of the polymers (i.e., the slopes of the lines in Figure 2a). We note that these values of the scaling factors apply to the polycations in the range of N we study (10−100 monomers); polyelectrolytes may show multiple scaling factors over a wider range of N. In the range of N we have studied, PCP-PolyX has a larger scaling factor than either PCO-PolyX or the linear architecture, suggesting that the grafted architecture with closer graft spacing has lower flexibility than the linear architecture or the grafted architecture with larger graft spacing. This trend is because closer graft spacing in PCP-PolyX leads to greater electrostatic repulsion between the charged oligolysine grafts. The scaling factors of uncharged polymers with the same architectures as the charged polycations show a universal decrease for all architectures (Figure 2b), clearly demonstrating that eliminating the charges leads to higher flexibility and smaller more compact conformations, which is expected because electrostatic repulsion is eliminated. Interestingly, the effects of both graft spacing and graft length on polycation size and flexibility are enhanced when charge is eliminated. Although uncharged PCP-PolyX has a smaller absolute radius of gyration than uncharged PCO-PolyX (Figure S6), the difference in the scaling factor is

dx.doi.org/10.1021/ma3011944 | Macromolecules 2012, 45, 8083−8096

greater than for the corresponding charged polycations, and the increase of the scaling factor with graft length is more pronounced. This is because in an uncharged state the polymers are smaller in size than in the charged state, and therefore excluded volume repulsion between grafts becomes more dominant within that compact state. When charges are present, the size of the polycation is closer to the contour length (i.e., the maximum possible size), and any further expansion must compete with lengthening the bonds comprising the backbone (Figure S7). The entropic unfavorability of maintaining a rod-like structure likely also plays a role. Therefore, the effects of the graft length and graft spacing on polycation size are lessened for the charged polycations compared to the uncharged polymers.

Polycation architecture has a substantial effect on the shape of the uncharged polymers and charged polycations, as quantified by the ratio of R_{ee}^2/R_g^2 in Figures 2c and 2d, respectively. In the case of the uncharged linear polymer, with an intrinsically stiff peptide backbone, R_{ee}^2/R_g^2 is near 12 for low N, indicating a rod-like shape, and decreases toward 6 for high N, indicating a globular polymer. The decrease occurs because at high N the length of the polymer backbone is greater than the persistence length of the peptide backbone. In contrast, the intrinsic flexibility of the polyolefin backbone of the uncharged grafted polymer leads to essentially globular behavior for all N studied here. Decreasing the graft spacing or increasing the graft length induces more rigidity, but the effect is minimal. The charged linear polycation behaves similar to the uncharged linear polymer, although it maintains more rod-like behavior at higher N due to electrostatic repulsion between charged monomers. The behavior of the charged grafted polymers is markedly different from their uncharged counterparts. First, for charged grafted polycations there is a shift from an essentially globular shape toward a more rod-like shape as N increases, in contrast with the globular shape at all N for uncharged grafted polymer. Second, increasing graft length increases the rod-like behavior, with the extent of increase decreasing with graft length. The graft spacing plays a weaker role in this overall shape factor because increased spacing increases both R_{ee}^2 and R_g^2, so the ratio is nearly the same regardless of graft spacing.

Next, we investigate in detail how polycation architecture affects global and local flexibility. The effect could be intrinsic (e.g., a rigid backbone) or architectural (e.g., induced by steric hindrance between grafts) or driven by electrostatics (e.g., due to like-charge repulsions).[21] Using the orientational correlation function, $\cos(\theta)^k$, as a metric of global flexibility, we see that the value of $\cos(\theta)^k$ for the uncharged linear polymer (Figure 3a) decays smoothly over a comparatively long distance (or length of the polymer) due to the intrinsic rigidity of the backbone. In contrast, for the uncharged grafted polymer the correlation decays over a shorter distance due to the intrinsically flexible polyolefin backbone, and the correlation shows no dependence on either graft length or graft spacing. The orientational correlation of the corresponding charged polymers (Figure 3b) decays over a longer distance than the uncharged polymers in all cases, indicating electrostatic repulsion-induced stiffness. One interesting behavior present in $\cos(\theta)^k$ for all of the polycations is the sharp decrease near the first and last monomers relative to the gradual decrease in the center. This inhomogeneity is attributable to end-effects: the monomers at the ends of the chain have greater free volume, thereby experiencing reduced repulsion from nearby monomers, and

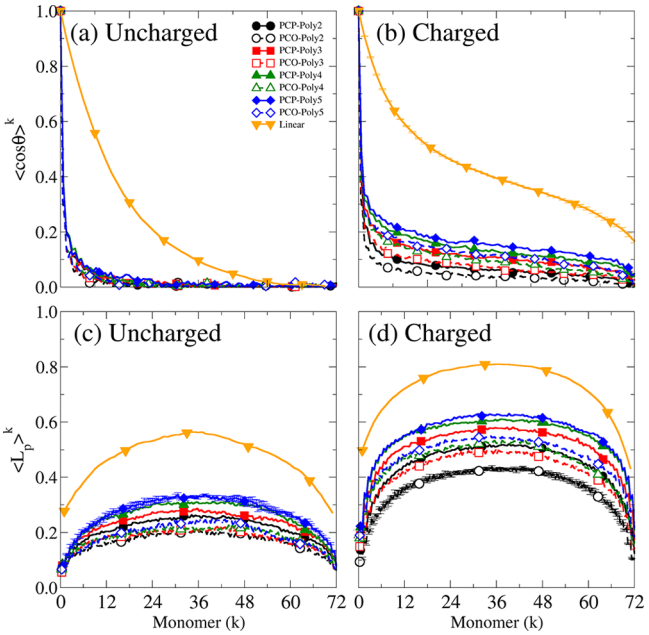

Figure 3. Effect of architecture and charge on polycation flexibility. The orientational correlation of uncharged polymers (a), and charged polycations (b), and the local orientational correlation of uncharged polymers (c), and charged polycations (d) as a function of monomer (k). All panels share the legend displayed in (a). Representative error bars are shown on only some lines for sake of clarity.

consequently they are more flexible.[42] The orientational correlation of the grafted polycations reveals slight increase in the stiffness with either increasing graft length or decreasing graft spacing, although the differences appear minor with this particular measure of flexibility.

The local orientational correlation function, L_P^k, is the correlation of each bond vector with the end-to-end vector of the polymer, yielding a metric of flexibility localized to each monomer. As with $\cos(\theta)^k$, the local orientational correlation typically takes on values between 0, indicating no correlation of that bond with the end-to-end distance and complete flexibility, and 1, indicating perfect alignment and complete rigidity. Figure 3c shows L_P^k for the uncharged polymers, and the observed trends are different than with the orientational correlation, $\cos(\theta)^k$. As with $\cos(\theta)^k$, the linear polymer is clearly more rigid locally than the grafted polymers, but what is not evident with $\cos(\theta)^k$ is a slight increase in local rigidity with increasing graft length or decreasing graft spacing. For the uncharged polymer, the effect of graft spacing is greater than the effect of graft length, with PCP-PolyX being universally more rigid than PCO-PolyX, even at the lowest graft length. Additionally, the polymer chain ends are more flexible than the central monomers, which is not apparent from the orientational correlation function (Figure 3a). As stated earlier, increased flexibility near the chain ends is attributable to their greater free volume and reduced steric hindrance by adjacent grafts. Figure 3d shows L_P^k for the corresponding charged polycations, and several of the same trends as observed for the uncharged polymers are evident. As with $\cos(\theta)^k$, the same increase in rigidity with increased graft length or decreased graft spacing is observed, although the differences are clearer with L_P^k. Compared to the uncharged polymers, two notable differences in the charged polycation L_P^k may be observed: first, the significance of graft length and graft spacing in determining the

dx.doi.org/10.1021/ma3011944 | Macromolecules 2012, 45, 8083−8096

local flexibility is increased, and second, the end effects are more dramatic, with greater differences between the central and end monomers in the charged case. The reason for both of these observations is that electrostatic interactions extend over a longer range than van der Waals repulsions (i.e., excluded volume), so that graft−graft repulsions in charged polycations extend over a longer range, and therefore electrostatic repulsion rises more sharply with increasing chain length than excluded volume effects. The local orientational correlation increases with graft length with the same asymptotic behavior as is observed for the shape factor R_{ee}^2/R_g^2 (i.e., the effect of increasing the graft length decreases with increasing graft length), which is sensible because the local rigidity defines the global shape.

To summarize the effects of architecture on the uncharged grafted polymers in the chain length range of 10−100 monomers, increasing graft length or decreasing graft spacing increases the size but has little effect on rigidity. Conversely, for the charged grafted polycations, increasing graft length increases the rigidity but has little effect on size, while increasing graft spacing decreases both the rigidity and the size scaling. These differences between the charged and uncharged molecules are due to the relative length scales and strength of electrostatic repulsion and excluded volume.

3.1.2. Effects of Ionic Strength and Counterion Valency. Having characterized the effect of polycation architecture and charge on structure with only neutralizing monovalent counterions, we now turn to the effects of both ionic strength and counterion valency. In addition to the simulations described in the previous section, which contained only the exact number of monovalent counterions necessary to neutralize the polycation charge, we have simulated the linear and grafted polycations at ionic strengths of 50 and 100 mM using either monovalent or divalent counterions as well as systems with only neutralizing divalent counterions.

Figure 4 shows the effect of ionic strength and counterion valency on the R_g scaling factor, ν, of the different polycation architectures. We note again that these scaling factors are extracted from simulations of grafted polycations in the chain length range of 10−100 monomers, and these polyelectrolytes may exhibit different scaling factors at larger length scales. As expected, increasing the ionic strength causes the polycations to become increasingly compact for all architectures, graft lengths, and graft spacings due to increased screening of the electrostatic repulsion between grafts.[43,44] As the ionic strength increases, the Debye screening length (i.e., the length scale of interactions between charged groups) is reduced. Similarly, by comparing Figures 4a and 4b, it is evident that increasing the counterion valency at a given ionic strength shrinks the polycations substantially: even with only neutralizing ionic strength, divalent counterions are more effective at compacting the polyelectrolyte, in agreement with some previous studies.[13,27,45]

The degree of contraction occurring with increasing ionic strength or counterion valency depends on the architecture. With monovalent counterions, the linear architecture is the smallest due to the shorter length of the backbone per monomer in comparison with the grafted architecture (i.e., 1 bead for linear, 2 for PCP-PolyX, and 3 for PCO-PolyX). However, with divalent counterions the linear architecture is intermediate in size between Poly2 and Poly5. This change occurs because divalent counterions are able to condense Poly2, with a fully flexible polyolefin backbone, more effectively than the linear polycation, which has a semiflexible peptide backbone.

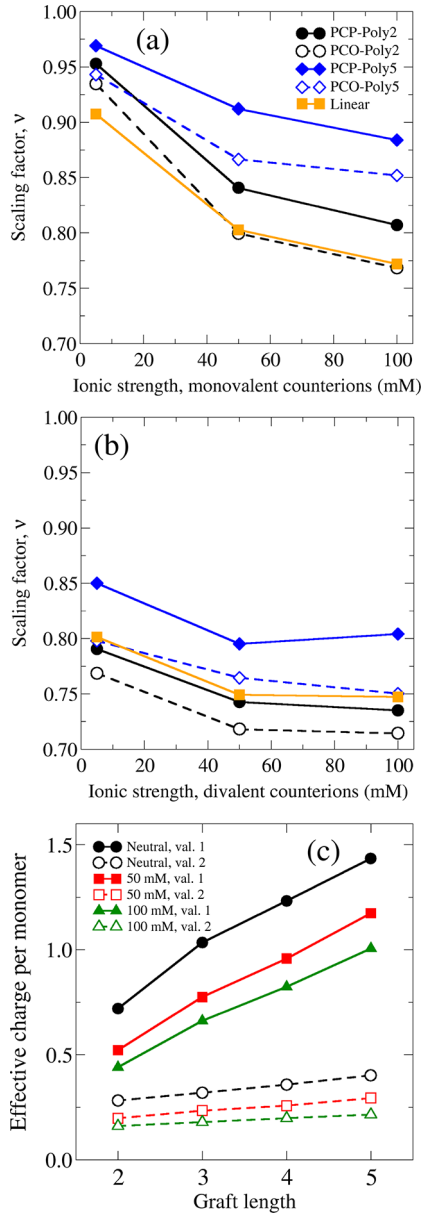

Figure 4. Effect of ionic strength and counterion valency on polycation size. Scaling factors for the relation $R_g \propto N^{\nu}$ at varying ionic strengths using (a) monovalent counterions and (b) divalent counterions. Only Poly2 and Poly5 are shown for the sake of clarity; the scaling factors of Poly3 and Poly4 are intermediate between the ones shown. Panels a and b share the same legend. Panel c shows the effective charge per monomer for PCP-PolyX, which is calculated by subtracting the charge of bound counterions from the charge per monomer. Short grafts are neutralized more effectively than long grafts as ionic strength or counterion valency is increased, leading to the smaller size of Poly2 compared to Poly5. PCO-PolyX is not shown because it is similar to PCP-PolyX.

For the grafted architecture at a given ionic strength and graft length, regardless of counterion valency, the scaling factor of PCP-PolyX is always higher than that of PCO-PolyX, due to increased graft−graft repulsion when the grafts are spaced more closely. With monovalent counterions, as the ionic strength increases, polycations with long grafts maintain a higher scaling factor, and the reduction in their scaling factor is lesser than

dx.doi.org/10.1021/ma3011944 | *Macromolecules* 2012, 45, 8083−8096

that of polycations with short grafts (Figure 4a). With divalent counterions, a similar trend is observed, although the decrease in the scaling factor is less dramatic than with monovalent counterions (Figure 4b). The reason for both of these trends is that the charge of Poly2 is neutralized more effectively than the charge of Poly5. Figure 4c shows the effective charge per monomer of PCP-PolyX, which is calculated by subtracting the charge of any counterions bound to a monomer from the total charge per monomer. Clearly, longer grafts maintain a higher effective charge than shorter grafts in all conditions, and this explains why Poly2 is condensed to a greater degree than Poly5 with increasing ionic strength. The higher effective charge per monomer results in higher effective graft−graft repulsion for longer grafts and therefore larger conformations. With divalent counterions, grafts of all lengths are mostly neutralized (effective charge near zero) even at the lowest ionic strengths, and the graft length has less of an effect on the effective charge than with monovalent counterions, which explains the reduced difference in size between Poly2 and Poly5 in the presence of divalent counterions.

To quantify the degree of counterion adsorption as a function of ionic strength and valency, we have calculated the number and fraction of counterions adsorbed to each individual monomer, as shown in Figure 5. Rather than examine the number of adsorbed counterions, which changes with the total number of counterions in the system and therefore in general does not allow for fair comparisons of different architectures, we present the fraction of counterions adsorbed to each monomer. The fraction of adsorbed counterions depends on the location of the monomer within the chain: monomers near the ends adsorb fewer counterions due to the lower electrostatic potential in those regions, as shown in Figure S8. Away from the ends of the polycation, the fraction of adsorbed counterions reaches a plateau value, due to the consistent electrostatic potential. In the following discussion, we will consider only the plateau value because it most simply represents the behavior of the polycations.

Figure 5a shows the plateau values for the fraction of adsorbed counterions for PCP-PolyX versus the graft length; PCO-PolyX is not shown because it is essentially similar to PCP-PolyX. Increasing the ionic strength increases the actual number of adsorbed counterions (Figure S8) but decreases the fraction of adsorbed counterions because of increased electrostatic screening. Also, since a given polycation can at most adsorb enough counterions to balance its charge, saturating the system with a large number of counterions will artificially lower the adsorbed fraction. Increasing the valency has the effect of dramatically increasing the fraction of adsorbed counterions for two reasons: first, there are a lower total number of divalent counterions required to reach a given ionic strength, and second, the adsorption of divalent counterions is more enthalpically favorable than the adsorption of monovalent counterions, while the entropic penalty for adsorption is the same. As the graft length increases, the fraction of adsorbed counterions monotonically increases. In the high ionic strength cases (50 and 100 mM) where the total number of counterions is identical for all graft lengths, the fraction adsorbed increases linearly with the length of the graft. However, in the neutral cases where the total number of counterions depends on the charge of the polycation (and hence on the graft length), the fraction adsorbed increase asymptotically because the total number of counterions also increases asymptotically: there are 2 times more counterions in the Poly3 systems than the Poly2 systems, only 1.5 times more counterions in the Poly4 systems than the Poly3 systems, and so on.

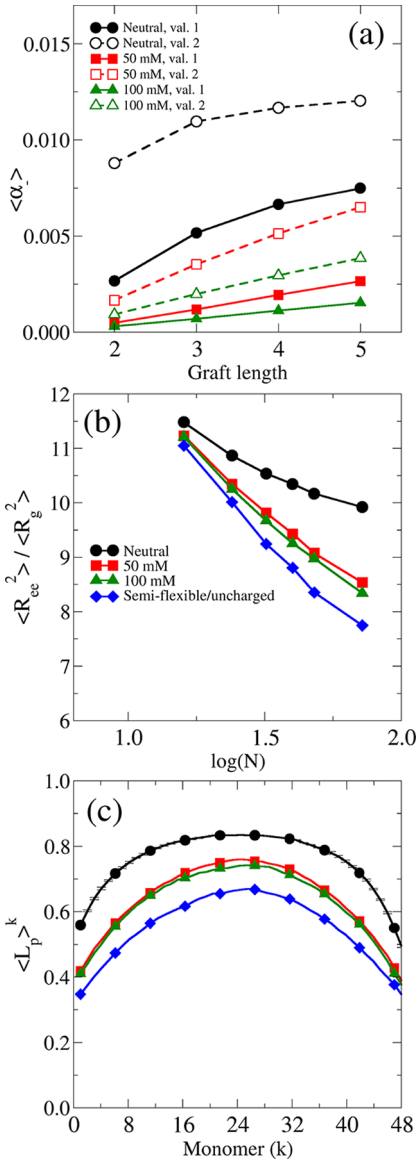

Figure 5. Effect of ionic strength and counterion valency on the fraction of adsorbed counterions and polycation structure. (a) The plateau values of the fraction of adsorbed counterions, $\langle\alpha_-\rangle$, as a function of graft length for PCP-PolyX. The trends for PCO-PolyX (not shown) are identical to those for PCP-PolyX. (b) Ratio $\langle R_{ee}^2\rangle/\langle R_g^2\rangle$ and (c) $\langle L_P\rangle^k$ for the linear polycation at various ionic strengths of monovalent counterions and the linear uncharged polymer. The grafted polycation is not shown because the general trends are the same as with the linear polycation. The trends for divalent counterions are similar but more pronounced. Panels b and c share the same legend.

The structural properties of the polycations are also affected by ionic strength and counterion valency. As the ionic strength is increased, the polycations become more globular, as evidenced by a decrease in the ratio R_{ee}^2/R_g^2 (Figure 5b). The polycations also become more flexible, as evidenced by a decrease in the local orientational correlation L_P^k (Figure 5c). All measures of polycation shape, size, and flexibility approach the values of the uncharged polymers as ionic strength or counterion valency is increased because the polycation charge is largely neutralized. Figures S9 and S10 contain additional data

dx.doi.org/10.1021/ma3011944 | Macromolecules 2012, 45, 8083−8096

on the shape and flexibility of the linear polycation, including the relative shape anisotropy and $\cos(\theta)^k$. Here, we only present results for the linear polycation because it shows the general behavior of all the polycations, and we only show results for monovalent counterions for clarity. The effects of increasing ionic strength with divalent counterions are more pronounced (Figures S9 and S10) because the polycations are more effectively neutralized by divalent ions, as is evident in Figures 4c and 5a. At high ionic strength with divalent counterions, the polycations behave like neutral polymers.

To summarize, the effect of increasing ionic strength or counterion valency is to increase screening between charges. Divalent counterions are substantially more effective at screening charges than monovalent counterions. Screening of charges causes the polycations to become increasingly compact for all architectures, graft lengths, and graft spacings, with the extent of compaction depending on the architecture of the polycation and the valency of counterions. Lastly, as the ionic strength is increased, the grafted and linear polycations become more globular.

3.2. Complexation of Linear Polyanions and Polycations. Having extensively characterized the behavior of the polycations in isolation, we now describe their interactions and behavior during polycation−polyanion complexation. We have performed a series of simulations at increasing ratios of positive to negative charge, termed in this work the charge ratio (CR). The charge ratio can differ from the nitrogen:phosphate (N/P) ratio that is typically used in the field of gene delivery in reference to the common chemical nature of the species involved (i.e., amines and phosphates). For the grafted architecture studied here, the charge ratio and N/P ratio differ because each grafted monomer has a total charge that is 1 less than the number of positively charged groups due to the presence of the negatively charged C-terminus group. We found that the charge ratio, not the N/P ratio, is what actually determines the nature of the polyelectrolyte complex; in fact, the N/P ratio produces misleading results (see Figure S11 for a representative example). We varied the charge ratio by changing the length of the polycation while maintaining constant polyanion length. To explore the effects of polyanion flexibility on the binding process, we have conducted two sets of simulations: one with a fully flexible polyanion and another with a semiflexible DNA-like polyanion. Initially, the polycation and polyanion are separated by some distance, and they condense into a polyplex during the course of the simulation. When characterizing the polyplexes, we consider only what we term the "polyplex region" (Figure 1e), which is the portions of the two polyelectrolytes that are within the Bjerrum length of one another. This distinction must be made because considering the entire structure of both polyelectrolytes could be misleading. An example is condensation at high charge ratios (CR > 1) when a large portion of the excess polycation may not interact with the polyanion at all, artificially increasing the apparent size and distorting the apparent shape of the polyplex if we did not consider only the "polyplex region".

First, we characterize the size and shape of the polyplexes. The effects of graft length, graft spacing, and charge ratio on R_g^2 of the polyplexes are shown in Figure 6. Here, we only consider the grafted architecture for simplicity. Generally, the linear polycation produces similar results to the grafted architecture, although the polyplexes tend to be larger and more anisotropic; results pertaining to the linear architecture are available in Supporting Information section 8. For the fully flexible

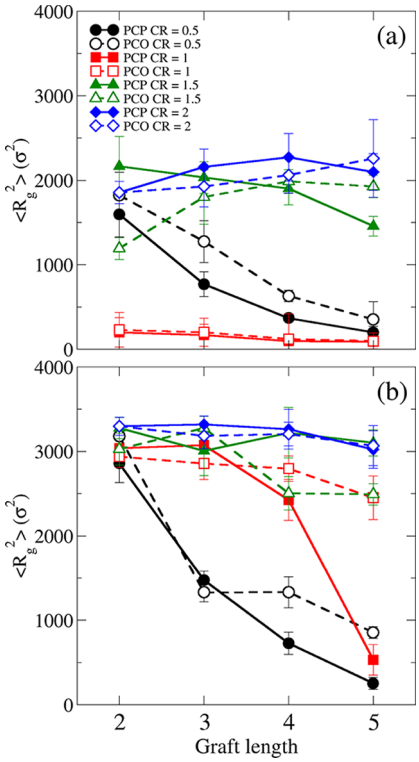

Figure 6. Effect of graft length, graft spacing, and charge ratio (CR) on polyplex size. $\langle R_g^2 \rangle$ for polyplexes formed by a polycation of the indicated graft spacing (PCP or PCO) and graft length (*x*-axis) with (a) a fully flexible polyanion and (b) a semiflexible, DNA-like polyanion. Both panels share the same legend.

polyanion (Figure 6a), the size of the polyplex is most sensitive to the charge ratio. At CR = 0.5, we observe that polycations with longer grafts are apparently able to condense the polyplex more effectively, regardless of the flexibility of the polyanion. However, this trend in size at CR = 0.5 is an artifact of the nature of the calculation and the relative lengths of the polycations involved: at a given charge ratio, Poly2 is 4 times longer than Poly5, and therefore the size of the region where the polycation and polyanion are in contact (the polyplex region) is larger for Poly2 than for Poly5. This artifact is not relevant at high charge ratios because then the length of the polyanion, which is constant, dictates the maximum size of the polyplex region. However, the results at CR = 0.5 is of little concern because the experimentally relevant range of charge ratios for polyanion condensation is CR $\geq$ 1, where our discussion of the results now continues. At charge neutrality (CR = 1), the polyplex collapses due to the lack of electrostatic repulsion. For CR > 1, the polyplex expands due to the excess positive charge. For the semiflexible polyanion (Figure 6b), the polyplex typically remains larger than any of the polyplexes formed with a fully flexible polyanion due to the added intrinsic rigidity in the polyanion. Notably, Poly5 is able to substantially condense the semiflexible polyanion at CR = 1, while the other architectures are incapable of this. This compaction occurs because Poly5 is substantially shorter than the polyanion at CR = 1, and it is therefore difficult to make favorable polycation−polyanion contacts if the polyanion is in an extended conformation. Poly5 exerts tension on the semiflexible polyanion until it forms a more compact structure that allows for a greater number of enthalpically favorable contacts. By contrast, the other grafted polycations are closer in length to

dx.doi.org/10.1021/ma3011944 | *Macromolecules* 2012, 45, 8083−8096

the polyanion at charge ratios near 1, so compaction of the polyanion is unnecessary to form favorable contacts.

The shape of the polyplexes, as quantified by the relative shape anisotropy (Figure 7), also depends on charge ratio,

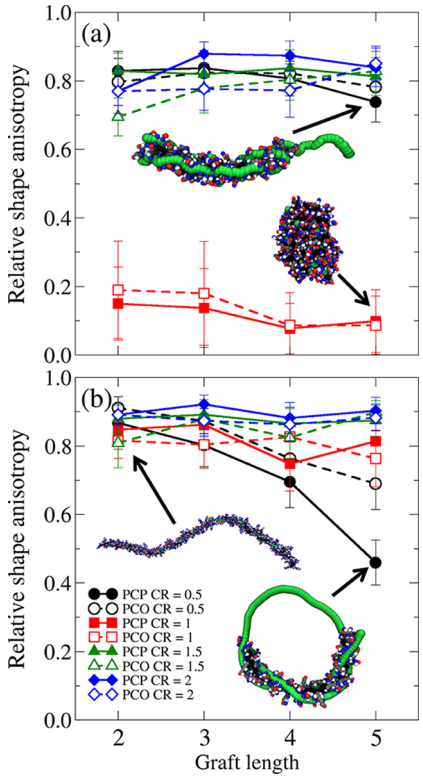

Figure 7. Effect of graft length, graft spacing, and charge ratio (CR) on polyplex shape. (a) Relative shape anisotropy of polyplexes formed between the indicated polycation architecture and a fully flexible polyanion. (b) Relative shape anisotropy of polyplexes formed between the indicated polycation architecture and a semiflexible polyanion, which could be considered a model for DNA. Representative snapshots of polyplex conformations are shown, with arrows indicating the corresponding value of the relative shape anisotropy. Both panels share the same legend.

architecture, and polyanion flexibility. The fully flexible polyanion (Figure 7a) is easily condensed into an isotropic globule at CR = 1, but the polyplex assumes an extended, anisotropic conformation for all other charge ratios. In the case of the semiflexible polyanion (Figure 7b), the polyplexes are never isotropic. Poly5, however, is capable of forming toroidal structures at CR = 0.5, which is evident upon visualization of the simulation trajectories (Figure 7b) and which appears as a decrease in the relative shape anisotropy.[37] The formation of toroids occurs for the same reason that Poly5 reduces R_g^2 at CR = 0.5, as discussed above. For CR > 1, the polyplex favors a rod-like conformation for all of the grafted polycations (Figure 7b): because the flexible grafted polycation can easily conform to the structure of the polyanion and the charge of the polyplex is inverted by the excess positive charge, the polyplex essentially behaves as a semiflexible polycation.

So far we have quantified the size and shape of the polyplexes as a function of polycation architecture and charge ratio. Next, we quantify the surface charge of the polyplex as a function of the same parameters. We quantify the surface charge by calculating the average total charge of counterions adsorbed to the polyplex region and dividing this quantity by the average surface area of the polyplex region. Because this quantity is defined in terms of counterions bound to the polyplex, it has opposite sign to the charge of the polyplex. We define a counterion as adsorbed to the polyplex if it is within the Bjerrum length of the polyplex region (i.e., those regions of the polyelectrolytes that are within the Bjerrum length of one another). Normalizing the charge of bound counterions to the surface area is necessary because increasing the surface area increases the available space for counterions to bind, and the surface area can depend on the particular conformation of the polyplex. An example of a polyplex conformation with lower surface area is a torus: since toroids typically involve multiple overlapping layers of the polyelectrolytes, a greater portion of the polyelectrolytes are buried within a dense polyplex region than would be in a rod-like conformation, thereby decreasing the surface area. The average total charge of adsorbed counterions and the polyplex surface area are available in Figures S15 and S16, respectively.

Figure 8 shows the adsorbed charge per surface area for the grafted polycation. In all cases, the surface charge decreases with charge ratio, being positive at CR < 1, neutral at CR = 1, and negative at CR > 1, which occurs because the increase in polycation length with increased charge ratio inverts the net charge of the polyplex. The surface charge displays interesting

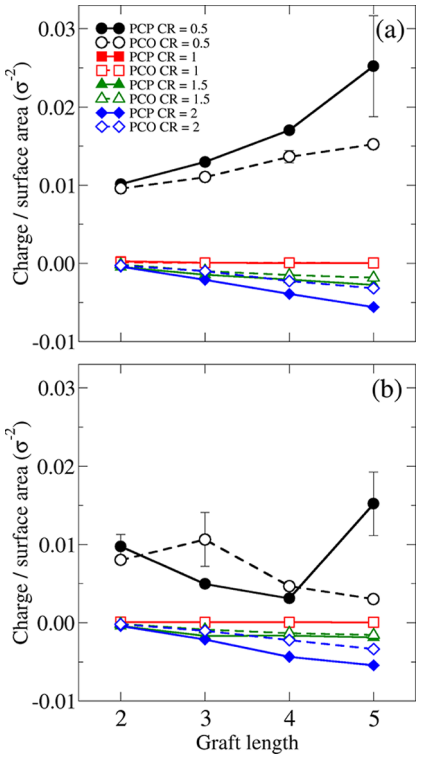

Figure 8. Effect of graft length, graft spacing, and charge ratio (CR) on the total charge of counterions adsorbed to the polyplex normalized to the surface area of the polyplex region for (a) the fully flexible polyanion and (b) the semiflexible polyanion. The total charge is calculated by summing the charge of all counterions that are within the Bjerrum length of the polyplex region, i.e., those portions of the polyelectrolytes that are within the Bjerrum length of each other. This quantity is a proxy for the polyplex surface charge, although of opposite sign because we are considering the counterions adsorbed to the polyplex surface. Both panels share the same legend.

dx.doi.org/10.1021/ma3011944 | *Macromolecules* 2012, 45, 8083−8096

polycation-dependent effects, which are most clearly evident for polyplexes formed with the fully flexible polyanion (Figure 8a): increasing the graft length or decreasing the graft spacing increases the magnitude of the polyplex surface charge. For the semiflexible polyanion (Figure 8b), the same trend is evident for CR $\geq$ 1, but an apparently nonmonotonic trend with graft length is evident for CR = 0.5. However, this trend is due to particular conformations taken on by polyplexes with the semiflexible polyanion. The semiflexible polyanion can form kinetically trapped structures, particularly with highly charged polycations such as PCP-Poly5, and the innate rigidity prevents rearrangement and redistribution of the polyplex charge. In contrast, the fully flexible polyanion can easily deform to accommodate the local geometry of the polyplex, ensuring consistent neutralization of the surface charge by evenly distributing the polyanion charge throughout the polyplex region. Regardless, the issue of kinetic trapping at CR = 0.5 is of little practical significance because experimentally relevant charge ratios are above charge neutrality (CR $\geq$ 1).

From a fundamental standpoint, the trends for the fully flexible polyanion are of interest (Figure 8a). The relatively short fully flexible polyanion simulated here could be considered a model for a semiflexible polyanion with a length substantially greater than the persistence length, like a long strand of DNA, since such a polyanion would be flexible over the length scale of the resulting polyplex. It may then be reasonable to extend the architecture-dependent results observed for these relatively small systems to larger scales. Therefore, the surface charge of polyplexes may be modulated by changing the linear charge density of the polycation, e.g., by changing the graft length or graft spacing for this particular architecture. Considering the importance of polyplex net charge and surface charge on DNA transfection efficiency, in particular, the ability of a polycation to impart a positive surface charge to the polyplex to allow favorable interactions with the cell membrane, it is interesting to find such architecture-dependent behavior.

4. CONCLUSIONS

Using Langevin dynamics simulations and coarse-grained models, we have studied linear poly(L-lysine) (PLL), poly(cyclopentene-*g*-oligolysine) (PCP-PolyX), and grafted poly(cyclooctene-*g*-oligolysine) (PCO-PolyX) to understand the combined effects of architecture and charge on the structure and flexibility of these lysine-based polycations. Comparing the linear and grafted polycations, we find that the linear polycation, although universally smaller than the grafted polycations with the same number of monomers, is universally more rod-like and less flexible than the grafted polycations, owing to the intrinsically rigid linear peptide backbone compared to the intrinsically flexible grafted polyolefin backbone. The same trend is observed for neutral polymers with the same architectures for the same reason. Considering only the grafted architecture, we find that increasing graft length or decreasing graft spacing increases the size and rigidity of the polycations, due to increased electrostatic repulsion between longer or more closely spaced grafts. The effect of increasing the graft length decreases as the graft length increases because each additional lysine added to a graft has a greater free volume and therefore repels adjacent grafts less effectively.

Interestingly, the size of the uncharged grafted polymers is more dependent on architecture (i.e., graft length and graft spacing) than the charged grafted polycations, while the rigidity of the charged grafted polycations is more dependent on architecture than the corresponding uncharged polymers. This reversal occurs because of the relative strength and length scales of excluded volume and electrostatic repulsion: excluded volume repulsion (i.e., Lennard-Jones repulsion) is weaker and acts over a shorter range than electrostatic repulsion. The uncharged polymers are smaller than the charged polycations so the effect of excluded volume is more prominent because the grafts are generally closer together. Increasing the graft length or decreasing the graft spacing increases the excluded volume repulsion between adjacent grafts, which in turn increases the size of the polymer. On the other hand, the size of the charged polycations already approaches the contour length (the maximum possible size) due to the electrostatic repulsion, and it is difficult to further expand the polycations because any further increase in size would compete with unfavorable lengthening of the bonds in the backbone. Therefore, increasing graft length or decreasing graft spacing produces weaker effects on the size of the charged polycations. The rigidity of the uncharged grafted polymers is lower than the charged grafted polycations due to the relative weakness of excluded volume repulsion, and the effects of graft length and graft spacing are lessened because of the shorter length scale of excluded volume: the polymer can bend substantially before distant monomers interact. The opposite is true when electrostatic repulsion dominates, leading to the greater rigidity and greater dependence of rigidity on graft length and graft spacing for the grafted polycations. These trends in rigidity and the molecular reasons for the varying rigidity with varying architecture can guide future chemical synthesis of linear/grafted polycations and in use of these polycations in applications other than gene delivery, such as in directing assembly of particles into nanostructures, as probes in biosensors, or drug delivery, where the flexibility of charged polymers/oligomers may play an important role.

We have also quantified the effect of ionic strength and counterion valency and find that increasing either value sufficiently will effectively neutralize the polycation and lead to behavior resembling the uncharged polymer, which results in a decrease in size and rigidity. Increasing the graft length or decreasing the graft spacing reduces the sensitivity to ionic strength and counterion valency because longer and more closely spaced grafts resist neutralization and maintain higher electrostatic repulsion between adjacent monomers, despite the fact that longer grafts adsorb a greater fraction of the total number of counterions. While past studies have shown that ionic strength and counterion valency can strongly affect the behavior of polyelectrolytes,[13,43] our work differs from previously published studies in that our polycation architectures are directly related to specific chemistries. By including details specific to the chemistries of the polycations we are modeling, we have been able to discern architecture-dependent properties beyond the general trends described in previous studies.

Polyplexes formed by complexation of these polycations with fully flexible and semiflexible linear polyanions exhibit sizes, shapes, and surface charges that depend strongly on the architecture and the charge ratio (CR) of the two polyelectrolytes. Polyplexes formed with a fully flexible polyanion at charge neutrality (CR = 1) are smaller and more globular compared to these polyplexes at CR > 1, which are larger and anisotropic. Polyplexes formed with the semiflexible polyanion maintain larger, more rod-like con-

formations than polyplexes formed with the fully flexible polyanion, except for the polycations possessing the longest grafts, which are capable of forming smaller toroidal polyplexes. The surface charge of the polyplexes is independent of the nature of the polyanion but depends strongly on the charge ratio and the architecture: at CR = 1, all polyplexes are neutralized, regardless of the graft length and graft spacing, whereas at CR > 1, increasing the linear charge density of the polycation, whether by increasing the graft length or decreasing the graft spacing, increases the surface positive charge of the polyplex. These results of the effect of linear charge density on surface charge density are particularly relevant for gene delivery and other biomedical applications because polyplexes must possess net-positive charge to interact favorably with the negatively charged cell membrane. Although it is not known how the magnitude of the polyplex charge affects transfection, the ability to tune surface charge may offer a route to improve transfection efficiency.

We have employed a simplified DNA-like polyanion model to study the fundamental behavior of these polycations complexing with polyanion. However, a more detailed DNA model may be required to accurately replicate polycation−DNA complexation. To this end, work to incorporate a more realistic model of DNA, with a level of detail comparable to our CG polycation models, is underway. Also, despite using coarse-grained models, the length scales in this study are smaller than the molecules studied experimentally. In experiments, plasmid−DNA with a length greater than 1000 base pairs is typically used, but the length of the DNA-like polyanion in this study is only 200 base pairs. Although the length of the polycations we have studied is comparable to the degree of polymerization used in experiments,[5−7] in experiments multiple such polycations are used to condense several strands of DNA into a polyplex, while only one such polycation is used here. Despite these limitations, this study serves as a good first step toward providing valuable guidelines as to how to modulate the polyplex charge, size, and shape by employing the appropriate graft length, graft spacing, and charge ratio: longer, more closely spaced grafts yield a higher surface charge than the converse, and higher charge ratios also lead to greater surface charge. Since a positive surface charge is requisite for transfection, one implication of these findings is that increased graft length may require lower polycation concentrations for efficient transfection, possibly reducing toxicity concerns in some applications. Most importantly, this work provides a fundamental understanding of how polycation architecture affects polycation structure and polyplex size and shape at various ionic strengths, which is useful not only for designing gene delivery agents but also for engineering ligands for bioseparations, flocculants, biocompatible coatings, and nanoparticle assembly.

■ ASSOCIATED CONTENT

Supporting Information

(1) Additional model details: polycation model design; (2) model calibration: linear polycation peptide backbone flexibility; (3) model calibration: grafted architecture polyolefin backbone hydrophobicity and flexibility; (4) additional model details and calibration: linear polyanion; (5) effect of architecture and charge on polycation structure; (6) effect of ionic strength and counterion valency; (7) N/P ratio produces misleading results compared to the charge ratio (CR); (8) linear architecture polyanion condensation results; (9) additional details on total charge of adsorbed counterions and polyplex surface area. This material is available free of charge via the Internet at http://pubs.acs.org.

■ AUTHOR INFORMATION

Corresponding Author

*E-mail arthi.jayaraman@colorado.edu; Ph (303) 492-3087; Fax (303) 492-4341.

Notes

The authors declare no competing financial interest.

■ ACKNOWLEDGMENTS

This research was partially supported by the National Science Foundation Award CBET-1066998 and TeraGrid resources provided by Kraken under Grant TG-MCB100140. This work also used the Janus supercomputer, which is supported by the National Science Foundation (Award CNS-0821794) and the University of Colorado Boulder.

■ REFERENCES

(1) Glover, D. J.; Lipps, H. J.; Jans, D. A. *Nat. Rev. Genet.* **2005**, *6* (4), 299−U29.
(2) Pack, D. W.; Hoffman, A. S.; Pun, S.; Stayton, P. S. *Nat. Rev. Drug Discovery* **2005**, *4* (7), 581−93.
(3) Boussif, O.; Lezoualc'h, F.; Zanta, M. A.; Mergny, M. D.; Scherman, D.; Demeneix, B.; Behr, J. P. *Proc. Natl. Acad. Sci. U. S. A.* **1995**, *92* (16), 7297−7297.
(4) Wagner, E.; Ogris, M.; Zauner, W. *Adv. Drug Delivery Rev.* **1998**, *30* (1−3), 97−113.
(5) Breitenkamp, R. B.; Ou, Z.; Breitenkamp, K.; Muthukumar, M.; Emrick, T. *Macromolecules* **2007**, *40* (21), 7617−7624.
(6) Breitenkamp, R. B.; Emrick, T. *Biomacromolecules* **2008**, *9* (9), 2495−500.
(7) Parelkar, S. S.; Chan-Seng, D.; Emrick, T. *Biomaterials* **2011**, *32* (9), 2432−2444.
(8) Wagner, E. *Proc. Natl. Acad. Sci. U. S. A.* **1991**, *88* (10), 4255−4259.
(9) Dennig, J.; Duncan, E. *Rev. Mol. Biotechnol.* **2002**, *90* (3−4), 339−347.
(10) Wang, Y.; Zheng, M.; Meng, F.; Zhang, J.; Peng, R.; Zhong, Z. *Biomacromolecules* **2011**, *12* (4), 1032−40.
(11) Mishra, S.; Webster, P.; Davis, M. E. *Eur. J. Cell Biol.* **2004**, *83* (3), 97−111.
(12) Elder, R. M.; Emrick, T.; Jayaraman, A. *Biomacromolecules* **2011**, *12* (11), 3870−3879.
(13) Ou, Z.; Muthukumar, M. *J. Chem. Phys.* **2005**, *123* (7), 074905−074905.
(14) Dias, R. S.; Linse, P.; Pais, A. A. C. C. *J. Comput. Chem.* **2011**, *32* (12), 2697−2707.
(15) Dias, R. S.; Pais, A. *Adv. Colloid Interface Sci.* **2010**, *158* (1−2), 48−62.
(16) Angelescu, D.; Vasilescu, M.; Staikos, G. *Colloid Polym. Sci.* **2011**, *289* (8), 871−879.
(17) Feuz, L.; Leermakers, F. A. M.; Textor, M.; Borisov, O. *Macromolecules* **2005**, *38* (21), 8891−8901.
(18) Bolisetty, S.; Airaud, C.; Xu, Y.; Müller, A. H. E.; Harnau, L.; Rosenfeldt, S.; Lindner, P.; Ballauff, M. *Phys. Rev. E: Stat. Phys., Plasmas, Fluids, Relat. Interdiscip. Top.* **2007**, *75* (4), 040803.
(19) Saariaho, M.; Ikkala, O.; Szleifer, I.; Erukhimovich, I.; ten Brinke, G. *J. Chem. Phys.* **1997**, *107* (8), 3267−3276.
(20) Kramarenko, E. Y.; Pevnaya, O. S.; Khokhlov, A. R. *J. Chem. Phys.* **2005**, *122* (8), 084902−10.
(21) Connolly, R.; Bellesia, G.; Timoshenko, E. G.; Kuznetsov, Y. A.; Elli, S.; Ganazzoli, F. *Macromolecules* **2005**, *38* (12), 5288−5299.
(22) Saariaho, M.; Szleifer, I.; Ikkala, O.; ten Brinke, G. *Macromol. Theory Simul.* **1998**, *7* (2), 211−216.

(23) Košovan, P.; Limpouchová, Z.; Procházka, K. *J. Phys. Chem. B* **2007**, *111* (29), 8605−8611.
(24) Borisov, O. V.; Zhulina, E. B. *Macromolecules* **2005**, *38* (6), 2506−2514.
(25) Cao, Q.; Zuo, C.; Li, L.; Yan, G. *Biomicrofluidics* **2011**, *5* (4), 044119−12.
(26) Cao, Q.; Zuo, C.; Li, L.; Zhang, N. *Macromol. Theory Simul.* **2010**, *19* (6), 298−308.
(27) Cao, Q.; Zuo, C.; Ma, Y.; Li, L.; Chen, S.; Hu, Z. *J. Polym. Sci., Part B: Polym. Phys.* **2011**, *49* (12), 882−889.
(28) Ou, Z.; Muthukumar, M. *J. Chem. Phys.* **2006**, *124* (15), 154902−154902.
(29) Narambuena, C. F.; Leiva, E. P. M.; Chávez-Páez, M.; Pérez, E. *Polymer* **2010**, *51* (14), 3293−3302.
(30) Cornell, W. D.; Cieplak, P.; Bayly, C. I.; Gould, I. R.; Merz, K. M.; Ferguson, D. M.; Spellmeyer, D. C.; Fox, T.; Caldwell, J. W.; Kollman, P. A. *J. Am. Chem. Soc.* **1995**, *117* (19), 5179−5197.
(31) Jorgensen, W. L.; Chandrasekhar, J.; Madura, J. D.; Impey, R. W.; Klein, M. L. *J. Chem. Phys.* **1983**, *79* (2), 926−935.
(32) Ullner, M. Polyelectrolytes. Physicochemical Aspects and Biological Significance. In *DNA Interactions with Polymers and Surfactants*; John Wiley & Sons, Inc.: New York, 2007; pp 1−39.
(33) Plimpton, S. *J. Comput. Phys.* **1995**, *117* (1), 1−19.
(34) Schlick, T. *Molecular Modeling and Simulation: an Interdisciplinary Guide*; Springer-Verlag: Berlin, 2002; Vol. *21*.
(35) Hockney, R. W.; Eastwood, J. W. *Computer Simulation Using Particles*; Taylor & Francis Group: New York, 1988.
(36) Rubinstein, M.; Colby, R. H. *Polymer Physics*; Oxford University Press: New York, 2008.
(37) Noguchi, H.; Yoshikawa, K. *J. Chem. Phys.* **1998**, *109* (12), 5070−5077.
(38) Mattice, W. L.; Suter, U. W. *Conformational Theory of Large Molecules: The Rotational Isomeric State Model in Macromolecular Systems*; John Wiley & Sons, Ltd.: New York, 1994.
(39) Dobrynin, A. V. *Macromolecules* **2005**, *38* (22), 9304−9314.
(40) Ullner, M.; Woodward, C. E. *Macromolecules* **2002**, *35* (4), 1437−1445.
(41) Humphrey, W.; Dalke, A.; Schulten, K. *J. Mol. Graphics Modell.* **1996**, *14* (1), 33−&.
(42) Limbach, H. *J. Chem. Phys.* **2001**, *114* (21), 9674.
(43) Kundagrami, A.; Muthukumar, M. *Macromolecules* **2010**, *43* (5), 2574−2581.
(44) Barrat, J. L.; Joanny, J. F. *Europhys. Lett.* **1993**, *24* (5), 333.
(45) Korolev, N.; Lyubartsev, A. P.; Nordenskiöld, L. *Adv. Colloid Interface Sci.* **2010**, *158* (1−2), 32−47.